Optimal observations for variational data assimilation

Armin Köhl and Detlef Stammer

Scripps Institution, La Jolla, California.

September 24, 2003

Short title: OPTIMAL OBSERVATIONS FOR VARIATIONAL DATA ASSIMILATION

Abstract. An important aspect of ocean state estimation is the design of an observing system that allows the efficient study of climate aspects in the ocean. A solution of the design problem is presented here in terms of optimal observations that emerge as nondimensionalized singular vectors of the modified data resolution matrix. The actual computation is feasible only for scalar quantities in the limit of large observational errors. In the framework of a 1° resolution North Atlantic primitive equation model it is demonstrated that such optimal observations when applied to determining the strength of the volume and heat transport across the Greenland-Scotland ridge, perform significantly better than traditional section data. On seasonal to inter-annual time-scales optimal observations are located primarily along the continental shelf and information about heat-transport, wind stress and stratification is being communicated via boundary waves and advective processes. On time-scales of about a month, sea surface height observations appear to be more efficient in reconstructing the cross-ridge heat transport than hydrographic observations. Optimal observations also provide a tool for understanding how the ocean state is effected by anomalies of integral quantities such as meridional heat transport.

1. Introduction

Through space born measurements and through global programs such as the Word Ocean Circulation Experiment (WOCE) and TOGA, we now have a data-rich environment which is unprecedented in the history of ocean research and includes altimetry (Fu and Cazenave, 2001) and a global profiling float program (ARGO; see Roemmich and Owens (2000)) as the backbone of a climate ocean observing system. However, to answer many scientific questions, our data base will remain insufficient (in time and space) and many quantitative climate studies must rely on a model-data synthesis (data assimilation) as a basis to compute observable and unobservable climate aspects. Among those are the variability of oceanic transport properties, of transport convergences, and other aspects of the large-scale circulation, such as changes of the meridional overturning circulation and its impact on climate. Required for climate studies are assimilation methods that are rigorous in a mathematical sense and take into account errors in data and the model alike without violating trustworthy dynamical principles. Among those approaches is that of the Pontryagian Principle, usually known as variational data assimilation, or the adjoint method.

The traditional use of the adjoint procedure in oceanography is that of a data synthesis. However, an important question with respect to a global synthesis is that of the design of an optimal observing system, i.e., the determination of the combination of various different observations and their geographical distribution that constrain ocean circulation models in a most effective way. Assessing an observing system in the context of the adjoint method is equivalent to assessing the impact of specific data types and their location on the convergence

rate of the optimization and to evaluating the sensitivity of the converged solution to additional data. Although any observing system design will therefore critically depend on the specific scientific question that lead to the formulation of the cost function, many features of the ocean's flow field are large scale, influencing climate through integral quantities. It is therefore hoped that any single basis for a climate observing system will impact many different climate aspects through the combination (in space and time) of ocean observations with model dynamics.

To date only a few studies exist that attempted an observing system design in a systematic way. Among those are Schröter and Wunsch (1986) who used the sensitivity of the cost function to determine the importance of specific data and Barth and Wunsch (1990) who employed a simulated annealing method for the configuration of an acoustic tomography array. The former approach is very similar to the one followed in the recent works of Marotzke et al. (1999) and Lee et al. (2002). Both publications suggest that the adjoint sensitivities of the heat transport to model state variables (e.g., temperature, salinity or velocity) may be used to identify regions in which hydrographic measurements or the knowledge of surface forcing are key for determining changes in the heat transport itself.

Adjoint sensitivities determine the relative importance of specific variables (e.g., wind stress or heat flux) on a cost function, such as meridional heat transport. However, those sensitivities do not take into account uncertainties in the observations or the model. For instance, anomalous heat transport could be caused by either kinematic or dynamic anomaly of the ocean state (Marotzke et al., 1999) or anomalous forcing conditions (Lee et al., 2002). The value of

adjoint sensitivities comes from the ability to predict the future evolution of the ocean state or, more specifically, certain aspect of transports, from observations collected in the past. For many cases it is, however, much easier to deduce transport anomalies from their effects on the ocean state. This classical hindcast situation is in general more important for oceanographic applications.

The purpose of this paper is therefore to discuss an observing system design that determines the observations that are most influential to the estimation of specific circulation aspects using the variational estimation approach. Although the method presented is generally derived, we focus in a first application on the determination of observations that in a model simulation allow us to monitor in a most effective way the Denmark Straight overflow and its cross-ridge heat transport.

Exchange processes across the Greenland-Scotland ridge (Hansen and Østerhus, 2000) are important for the determination of hydrographic conditions south and north of the sills and more generally the maintenance of the meridional overturning circulation (MOC). The Denmark Strait Overflow Water (DSOW) and Island Scotland Overflow Water (ISOW) contributes to the formation of North Atlantic Deep Water (NADW) that moves equator ward at depth and affects the thermohaline structure of the global ocean. Although the role of the Greenland-Iceland-Scotland (GIN) Sea in NADW formation and in determining our present and future climate seems to be widely accepted (Dickson and Brown, 1994), a detailed understanding of (1) the degree of transport variations and (2) adjustment processes of the flow over the Greenland-Scotland ridge (GSR) to changing forcing conditions over the GIN

Sea has not yet been established. However, several indications exist for longterm changes of the overflow characteristics and of the hydrography in the adjacent regions (Dickson et al., 2002; Bacon, 1998; Hansen et al., 2001). Biastoch et al. (2002) discuss the sensitivity of that transport to changes in wind forcing over the sub-polar gyre and to cross-ridge density gradients. We here determine in a model simulation the observational data base required to monitor changes of transports across Greenland-Scotland ridge.

The structure of the paper is as follows: Section 2 explains the concept of optimal observations; the model framework in which the concept will be applied is summarized in Section 3. In Section 4 we discuss the inter-annual to decadel variability of the cross-ridge transports as they follow from a 50-year long model simulation. In Section 5 a set of observations is then constructed that are required to determine those changes in a best possible way. In Section 6 the efficiency of optimal data distribution is finally tested in an assimilation experiment and the relative importance of different observational variables is discussed in Section 7.

2. The concept of optimal observations

To introduce the notation we will start with a brief summary of variational data assimilation and then provide a compact description of optimal observations, i.e., observations which constrain a model in an optimal way. For a detailed account on inverse modeling in oceanography see Wunsch (1996) and Fukumori (2001).

Define an ocean general circulation model (OGCM) as

$$\frac{\partial x}{\partial t} = f(x, \alpha),$$ (1)

where x is the model state, and α is a vector of control parameters. Observations are related to the model state through the observational matrix **E** as

$$y = \mathbf{E}x + n,$$ (2)

where n is the noise in the observations. In essence, the estimation procedure finds control parameters (α) that are required to bring the model trajectory into consistency with noisy observations and with an imperfect model. Those control parameters usually include uncertain quantities such as the model initial conditions, surface and lateral boundary conditions, or model mixing parameters.

To proceed, we linearize the model (1) around the a priori set of control parameters, α^o. The dependency of changes of the trajectory δx of to changes $\delta\alpha$ may then be represented in a compact notation as

$$\delta x = \mathbf{F}\delta\alpha.$$ (3)

Kleeman and Moore (1997) show in their introduction to the derivation of stochastic optimals how one can go from a classical parabolic form (1) to this compact notation. Here $\delta\alpha = \alpha - \alpha^o$, $\delta x = x - x^o$, and x^o is the model trajectory for the set of control parameters α^o. Changes in $\delta\alpha$, δx and δy are assumed here to be small. Similar to a linear propagator, F is not a local (in time and space) operator, but involves convolutions of $\delta\alpha$ in space and time. For almost all applications of ocean state estimation that involve a full nonlinear OGCM this kind

of relation is too complex to be provided in a complete form. Stammer and Wunsch (1996) provide an application in which an approximation of $\mathbf{F}$ is explicitly calculated.

The parameter improvement $\delta\alpha$ might in principle be written in terms of the observations y or, equivalently, the initial model data difference

$$\delta y = y - \mathbf{E}x^o, \tag{4}$$

The relation

$$\delta\alpha = \mathbf{B}\delta y, \tag{5}$$

is the solution of the optimization problem which minimizes the norm of δy under further constraints and which is given in a more explicit form below. By combining (5) with (3), a linear mapping from the observational space onto the space of model trajectories,

$$\delta x = \mathbf{FB}\delta y = \mathbf{A}\delta y, \tag{6}$$

is obtained. The modified data resolution matrix $\mathbf{A}$ ($\mathbf{EA}$ would be the true data resolution matrix) to maps observations, expressed as model-data differences onto trajectory improvements of the model. It projects the information of the ocean on the state or change of state as far as it is included in the model dynamics. Menke (1989) already proposed the matrix as a useful tool in experimental design.

Optimal observation locations are described accordingly by the nondimensionalized singular vectors of the resolution matrix $\mathbf{A}$. Optimal means in this respect that these observations would induce maximal changes of the trajectory δx when assimilated in a variational assimilation system.

Calculating singular vectors of $\mathbf{A} = \mathbf{FB}$ in the generality of the last paragraph is prohibitive in the context of a full nonlinear OGCM. We therefore restrict our further applications to cases where the model state is projected onto a single scalar quantity, $h(x)$, such as meridional heat transport in the ocean. Then the dependency of h on the data y can be described by the gradient $\partial h/\partial y$ itself. This gradient can be written as the product of two terms,

$$\frac{\partial h}{\partial y} = \frac{\partial h}{\partial \alpha}\frac{\partial \alpha}{\partial y}; \tag{7}$$

both will be treated separately in the following.

In the same way as the adjoint operator $\mathbf{F}^+$ is used in the adjoint model to calculate gradients of the cost function with respect to the parameter α, the first term

$$\left(\frac{\partial h}{\partial \alpha}\right)^T = \left(\frac{\partial h}{\partial x}\frac{\partial x}{\partial \alpha}\right)^T = \mathbf{F}^+\frac{\partial h}{\partial x} \tag{8}$$

can be calculated by replacing the cost function with h. Note that $\partial h/\partial x$ is in general a simple relation which does not involve the integration of any dynamical model.

In order to approximate the second part, a more explicit expression for the inverse relation (5) is required. With $\mathbf{W}$ and $\mathbf{V}$ describing the weight, i.e., inverse of the error covariance of the data and the parameter, the cost function can be written as

$$J = \frac{1}{2}(\delta\alpha)^T\mathbf{V}\delta\alpha + \frac{1}{2}(y - \mathbf{E}x)^T\mathbf{W}(y - \mathbf{E}x) + \lambda(\delta x - \mathbf{F}\delta\alpha); \tag{9}$$

where we made use of the linearized version (3) of the model. A general solution to minimizing (9) can be written as

$$\delta\alpha = \mathbf{V}^{-1}\mathbf{F}^+\mathbf{E}^+(\mathbf{W}^{-1} + \mathbf{E}\mathbf{F}\mathbf{V}^{-1}\mathbf{F}^+\mathbf{E}^+)^{-1}\delta y. \tag{10}$$

(see Menke (1989)). For most applications the term $\mathbf{W}^{-1}$ can be assumed to be smaller than $\mathbf{EFV}^{-1}\mathbf{F}^{+}\mathbf{E}^{+}$, i.e., data are relatively accurate as compared to the model (note that $\mathbf{W}$ is the inverse observational error covariance), the observations would otherwise not improve the state. We however postulate to the contrary that $\mathbf{EFV}^{-1}\mathbf{F}^{+}\mathbf{E}^{+}$ can be neglected in comparison to $\mathbf{W}^{-1}$, i.e.. The relation (10) is thus evaluated for the limit of large observational errors which is in accord with our initial assumption: that the new state is close to the first guess x^{o}. While this assumption is made in order to allow for a considerable simplification its justification is given below by testing the estimated data distribution in identical twin experiments. With the latter approximation, Eq. 10 reduces to

$$\delta\alpha = \mathbf{V}^{-1}\mathbf{F}^{+}\mathbf{E}^{+}\mathbf{W}\delta y \tag{11}$$

We note that Eq. 11 does not involve a full inversion of the model, but the calculation of weighted forcing anomalies from one backward calculation of the adjoint model $\mathbf{F}^{+}$ driven by the weighted model-data differences $\mathbf{W}\delta y$.

Combining Eq. 11 with Eq. 8 yield the final result

$$\left(\frac{\partial h}{\partial y}\right)^{T} = \mathbf{WFV}^{-1}\left(\mathbf{F}^{+}\frac{\partial h}{\partial x}\right)^{T}. \tag{12}$$

This relation involves the adjoint $\mathbf{F}^{+}$ and a linearized version $\mathbf{F}$ of the forward model. The construction of a linearized model is a similar effort as the construction of an adjoint. However, this step can be avoided by a finite difference approach. The procedure starts with a forward run and the application of one optimization step employing the gradient $\mathbf{F}^{+}\partial h/\partial x$ calculated by the adjoint to reduce h. The optimization step requires a normalization that

involves naturally the weight V of the control parameter. The step-size of the parameter innovation $\delta\alpha$ should be small enough to keep the trajectory of the second forward model run with the new parameter set in the vicinity of the trajectory corresponding to the initial forward run. The difference of the two trajectories approximates the trajectory of the linearized model F. After scaling with the weight W^+, this difference is proportional to $\partial h/\partial y$ in case E equals the identity. In summary, the calculation of optimal observations involves in principle a single iteration of variational assimilation procedure. It is a necessary condition that the cost function h is actually reduced during this step which is however in general guaranteed for a small enough step-size.

Optimal observations were chosen to affect the quantity of interest, h, maximally when used in a variational data assimilation system i.e., adding observations at those locations will reduce uncertainty of h. Since most OGCM have model output like temperature and salinity fields in physical units, a weighting or normalization is necessary before a data type or an observational site can be inferred from the spatial structure of the gradient.

This does not necessarily imply that the quantity of interest is estimated with the greatest exactness, which would certainly be the ultimate criterion for selecting observations. If all observations are available and precise enough to define h from measurements alone, it would be the best way to estimate h directly without using any assimilation system. Optimal observations defined by the maximum gradient criterion are preferable in cases where measurement errors are large and where only sparse data sampling either in time or space is affordable. This is in accord with the approximation that the error of the observations is large

in comparison with the error of the parameters.

Preferred data locations are identified by the extreme values of the gradient $\partial h/\partial y$. We note from Eq. 12 that the spatial structure of the gradient is not affected by the ratio of the weights V to W. The result (in contrast to the derivation) is thus not sensitive with respect to the validity of the assumption of large observational errors. However, the relative error of data types (e.g. temperature vs. salinity) or of certain parameters (e.g. wind stress vs. heat flux) is of profound importance as it directly affects the importance of certain data types. Most data assimilation experiments use weights that violate our assumption. In principle one may multiply W by a small number and use the estimated optimal observations as an approximation. Since spatial patterns are not affected, we choose in the following section a priori weights disregarding their ratio.

3. Model framework

The design of optimal observations and the evaluation of the performance in a variational assimilation system requires all components necessary for ocean state estimate, i.e., the forward model, its adjoint, the model-data interface and an optimization procedure. The physical model was developed at the Massachusetts Institute of Technology (MIT) and is described by Marshall et al. (1997). It is based on the primitive equations in a z-coordinate formulation and is operated here in a hydrostatic mode with an implicit free surface and partial bottom cells implemented (see Adcroft et al. (1997) for details). The MIT model code is designed to allow the construction of the adjoint using the automatic differentiation tool

TAMC (Giering and Kaminski, 1998). Marotzke et al. (1999) describe in detail the MIT adjoint model generation. Stammer et al. (2002a,b,c) describe a first global state estimation attempt with this model. The Quasi-Newton optimization algorithm is described by Gilbert and Lemaréchal (1989).

The model used in this study covers the North Atlantic Ocean from 20° S to 76° N with realistic topography based on the ETOPO5 (1988) dataset. The spatial resolution is 1° in longitude and $1^o \cos \phi$ in latitude. The thickness of the 37 vertical levels increases smoothly from 11m at the surface to 250 m below 1000m. Closed northern and southern boundaries as well as the Strait of Gibraltar have a 5° restoring zone attached in which potential temperature and salinity is relaxed toward monthly mean values of Levitus et al. (1994). Horizontal and vertical viscosity is parameterized by Laplacian mixing with values of 10^4 m^2 s^{-1} and 10^{-3} m^2 s^{-1}, respectively. The horizontal diffusivity is set to 10^3 m^2 s^{-1}; in the vertical a Laplacian diffusivity of 10^{-3} m^2 s^{-1} was prescribed in combination with a convective adjustment scheme.

The model was forced with once per day surface heat and virtual salt fluxes as provided by the National Center for Environmental Prediction (NCEP)/National Center for Atmospheric Research (NCAR) re-analysis project. Daily short wave heat-flux is prescribed separately from turbulent heat flux contributions; its vertical profile of absorption is modeled by the analytical formula of Paulson and Simpson (1977) for prescribed time dependent ocean water types after Jerlov (1968). An additional relaxation term is introduced to relax surface temperature and surface salinity towards the monthly mean values of the climatology with a 30-day time-scale.

Wind stress fields are twice per day.

Eq. 9 requires prior information about data and model errors. The weights $\mathbf{W}$ and $\mathbf{V}$ are approximated by the error profiles for temperature and salinity taken from Levitus et al. (1994). Error values for the surface forcing fields were assumed to be constant in space and time and were given values of 100 W/m^2, 1×10^{-7} m/s and 0.05 N/m^2 for the heat-flux, salinity flux and wind stress, respectively.

The model was started in January 1948 from rest with initial conditions for temperature and salinity taken from Levitus et al. (1994) and integrated for 50 yrs driven by NCEP reanalysis fluxes at the surface. Years with specifically high or low transport values were selected from this reference run to serve as data in identical twin experiments. The set of control parameters in all our experiments comprises initial conditions for temperature and salinity and monthly mean corrections for the forcing fields. All experiments as well as the calculation of optimal observations were carried out over a period of the year 1990.

4. Greenland Scotland ridge transports simulations

In the next sections we will analyze observations that are required to optimally determine variations of GSR transport variations. But before we do so, we will provide first a description of transport variations as they occur in the 50 year long model simulation and discuss underlying physical mechanisms.

The flow through Denmark Strait (DS) and the subsequently down slope flow along the topography depend on processes that are not sufficiently resolved in most models and are

essentially absent in our 1° version of the MIT model. Specifically, the MIT Z-coordinate model represents the downward flow by consecutive convective adjustment steps which entails substantial mixing. Water masses are therefore not conserved downstream of the sill and a realistic hydraulic control overflow mechanism is absent. However, the wind-driven barotropic cross-ridge transport may still be realistic (Biastoch et al., 2002). For the present model an estimated time-mean barotropic transport through DS strait at 65.4°N of 4 Sv agrees well with results from Käse and Oschlies (2000) (also 4 Sv).

Fig. 1 shows that the GS ridge heat transport variability is closely linked to the

atmospheric variability as described by the North Atlantic Oscillation (NAO) index (i.e.,

the difference of normalized sea level pressures (SLP) between Ponta Delgada, Azores and

Stykkisholmur/Reykjavik, Iceland; see Hurell and van Loon (1997) for details). A high NAO

index is associated with stronger-than-average westerlies over the mid latitudes. It thus leads

to an enhancement negative wind stress curl over the sub-polar North Atlantic that in turn

drives an anomalous barotropic circulation around Island (Biastoch et al., 2002), and thus

determines the southward transport variability through DS.

<div style="float:right; border:1px solid black; padding:4px;">Fig. 1</div>

Net southward volume transport through the DS is compensated by the northward volume flux of warm water over the ridges east of the strait. Anomalies of the southward volume transport through DS and the net heat transport over the GSR are thus strongly correlated. The maximum correlation between the NAO index and the GSR heat transport as displayed in Fig. 1 is 0.80 and shows no lag in time, whereas the correlation with DS volume transport is lower (0.70) with a slight positive lag of about 5 months.

Fig. 1 indicates that NAO variability has spectral power in the decadel band and in the inter-decadel band on periods longer than 50 years The transport curves show less inter-decadel variability but are noticeably affected by the decadel-scale atmospheric variations. In contrast, an inter-decadel signal clearly dominates the time-series of temperatures that are being advected across the GSR. They are shown in Fig. 2 and represent basin-averaged temperature [Fig. 2] anomalies north and south of the sills. While a decadel signal is visible in the northern time-series, the southern basin varies primarily on inter decadel time scale. We note that both curves show distinct lags with respect to the NAO index, with the temperature south and north of the sill leading and lagging the NAO index by approximately 4 years, respectively.

The basin-averaged temperature is affected by surface heat fluxes. The figure suggests, however, that the basin-averaged temperature anomalies to some extent are actually also an integrative consequence of anomalous cross-ridge heat transport, even on inter-decadel time scales: Persistently lower than normal southern temperatures have the tendency to lead to decreased northward heat transports that in turn leads to decreasing temperatures north of the ridge. This interpretation is important for an observing system design: anomalous cross-ridge heat transports create water mass anomalies that are subsequently carried around advectively in individual basins by the circulation. Observations located remote from the ridge have thus the potential to record the history of the heat transport across the ridge.

5. Optimal observations for the February GSR heat transport

What needs to be measured in the ocean to reconstruct the heat transport variations across the GSR ridge that were described in the previous section? To answer this question we use the concept of optimal observations with the the scalar h representing the February 1990 heat transport across the GSR.

In previous publications only adjoint sensitivities were used to obtain insight into an observing system design (e.g. Marotzke et al. (1999); Lee et al. (2002); Schröter and Wunsch (1986)). Sensitivities of the February cross-ridge heat transport with respect to the January 1st temperature and salinity initial conditions are shown in Fig. 3. The figures show a positive- $\boxed{\text{Fig. 3}}$ negative sensitivity pattern for temperature and salinity between Iceland and Scotland which lead to consistent dynamic density anomalies. They both support an enhanced northward volume flux into the Norwegian Sea and thus an enhanced cross-ridge heat transport. In contrast, the pattern of negative sensitivity north of Iceland is only visible in temperature which is passively advected though the DS.

Optimal observations are the gradient of the GSR ridge heat transport with respect to monthly mean temperature observations. They are shown for selected months of a one-year period in Fig. 4. At the beginning of the assimilation period the distribution of optimal observations is $\boxed{\text{Fig. 4}}$ similar to the sensitivities shown in the previous figure. However, in February the signal of cold overflow emerges in the DS and starts to descend south of it in later months. The vertical mixing process and the descent to its final depth is also visible for the following month as a negative gradient gradually approaching deeper layers. In accord with the enhancement of

a barotropic cyclonic gyre around Iceland that was discussed above, the cold DS signal is associated with an enhanced cross-ridge heat transport. The same is true for less southward IS overflow water which is documented by the positive gradient south of Iceland. The fact that the patterns are south and not north of the sill documents that there no net northward flow through this strait. Negative gradients close to Scotland are due to a local wind driven overturning cell east of Iceland.

If one were to compute the December heat transport, sensitivities could then be calculated for all months of the year similar to Schröter and Wunsch (1986), but they would still differ from optimal observations since the latter reflects only the influence of possible changes in the forcing fields and in the January initial conditions, whereas adjoint sensitivities describe the influence of many arbitrary changes of the hydrography that may or many not be realistic changes in forcing fields and initial conditions in January.

Optimal observations are related to adjoint sensitivities as given by Eq. 12: they are adjoint sensitivities which are weighted by observational and model error matrices, i.e. (W) and (V) and propagated by the linearized forward model. Therefore, adjoint sensitivities describe only the causes of anomalies, whereas optimized observations blend causes and effects. For January, both fields show similar patterns along the eastern boundary, however optimal observations emphasize the deeper layers due to the nondimensionalisation of the gradient. The distributions of optimal observations for the period after February are determined by the cross-ridge heat transport anomalies and subsequent advective processes.

Optimal observation sites are very rare in January but accumulate toward the end of the year.

This is because hydrographic measurements taken in December are influenced by the flow field throughout the entire year and thus provide maximum information about wind stress anomalies that in turn influence the cross-ridge heat and volume transports in February. January temperature anomalies influence the February cross-ridge heat transport kinematically and provide only little (or no) information about the wind stress forcing field. January density anomalies are of dynamical importance for they enhance the inflow into the Norwegian Sea but the advective effect on the hydrography carries more important information about the cross-ridge transports. Because of the dominant control by wind-stress conditions, the GS ridge heat transport has a large component that is not predictable from kinematics alone (in contrast to the suggestion of Marotzke et al. (1999) for the heat transport at 29°N).

6. Reconstruction of the GSR heat transport

In the previous section we discussed the distribution of optimal observations and their relation to physical mechanisms in the ocean. Here we will now provide a "proof of concept" by demonstrating that optimal observations are indeed most efficient in reconstructing the GS ridge heat transport. To that end, hydrographic model fields taken from year 1990 serve as simulated data. The cost function is proportional to the quadratic model-data misfit of temperature and salinity at the respective positions where observations exist and will be minimized with the adjoint method. The assimilation period for all experiments is one year. The control parameter set for the variational assimilation system comprises initial hydrographic conditions and monthly mean correction for the surface flux fields. The first

guess for the forcing and initial conditions were taken from model year 1965. The goal of the experiments is to reconstruct the heat transport across the GSR in 1990. The years 1965 and 1990 were selected since they represent extreme conditions of anomalous low and high GSR heat transport values (compare Fig. 1).

We will discuss in this section the success of reconstructing the GS ridge heat transport based on three different data distributions: (1) T,S over the ridge only as it would be the case for a hydrographic section. (2) Optimal observations of T and S observations which in most cases are located away from the location where the heat transport is being estimated. (3) T and S on the full model grid (only for the case of reconstructing February heat transport). To enable a quantitative comparison, the number of hydrographic data at optimal locations was chosen to be the same as the number of data in the section.

In Fig. 5 we plot the difference between the true 1990 model heat transport and the reconstructed 1990 annual mean heat transport against the quadratic model data misfit of the hydrographic observations. Results are provided for the two above data distributions: (1) and (2). Since each symbol represents individual iterations of the optimizations, the convergence rate of the optimization towards the true heat transport can be inferred from the curves as well. Both data distributions have skill in reconstructing 1990 annual mean heat transport. But the significantly larger initial model-data misfit in case (2) indicates already the larger sensitivity of the system to optimal observations which subsequentially allows reconstruction of the annual-mean heat transport almost perfectly for this data distribution after only about 10 iterations.

| Fig. 5 |

Analyzing the temporal evolution of the reconstructed 1990 heat transport (not shown) it becomes clear that the temporal heat transport fluctuations are not constrained at all by both previous data distributions, but still reflect the 1965 conditions. The largest discrepancy actually occurs during February, despite the fact that the annual mean heat transport was recovered successfully. To understand this puzzle, we investigate next whether a data distribution can be found at all that allows reconstructing of the heat transport for an individual month — taken here to be February 1990 — or if some systematic difficulty prevents the reconstruction of the circulation on shorter time-scales.

Fig. 6 shows the heat transport error as a function of the cost function value for the two different experiments corresponding to (1) an optimal data distribution (compare Fig. 4) and (2) monthly mean temperature and salinity data available on the full model grid available for the 12 month period. Several findings are noteworthy from the figure. Firstly, an optimal data distribution performs better than a complete temperature and salinity distribution. Moreover, in both cases the cross-ridge heat transport can not be reconstructed successfully - in striking contrast to the previous annual-mean case. The heat transport error is reduced by more than 50% after assimilating optimal data. However, since the target value of year 1990 was anomalous high and the value corresponding to the first guess was anomalous low, the actual skill for the reconstructing of monthly mean heat transport is still quite low. The surprising degradation of the result upon the usage of basin-wide data coverage is likely due to the fact that most of the additional data do not contain any extra information about the heat transport, but at the same time, lead to a more complex structure of the cost function. Further

improvement might be possible with additional iterations, though.

To understand the failure of reconstructing the heat transport, we performed an experiment that did not use convective adjustment. For the latter case, all data and heat transport values to compare with are taken from a year 1990 experiment without convection. Optimal locations were specifically calculated for a set-up without convection. As Fig. 6 indicates, the remaining error of the heat transport is reduced to less than 40% and the simultaneous reduction of the cost function suggest a closer link between hydrographic data and cross-ridge transports than was obvious previously with convective adjustment.

Convective adjustment plays an important role in the forward model where it transports the overflow signal toward depth. The same convection process transports the model data misfit information of the overflow signal back to shallow depth and enables the estimation of surface wind stress corrections. However, this is true, only if overflow and convection takes place in the forward run around which the adjoint is linearized. The first guess simulation uses 1965 forcing which leads to low February heat transport and is characterized by almost no overflow and thus no convection in February. Due to the lack of the process that transports the information to the surface the signal about the February 1990 overflow remains hidden at depth. This is a general problem of the linearization approach of the adjoint method. Nevertheless, optimal observations shown in Fig. 4 still give the correct locations since the construction uses a finite difference approximation instead of the linearized forward model. This problem has less influence on the estimation on longer time-scales (as with the annual mean). High heat transport variability ensures the existent of convection events. Convectively

driven mixing renders T and S observations less effective (see also discussion in the next section) for the estimation of the cross-ridge heat transport. This might also be true for state estimations in general.

7. SSH vs hydrographic data

The close relation between GSR heat transport variability and the wind stress curl variability (Biastoch et al., 2002) around Iceland shows that the success of transport estimations mainly depends on the ability to estimate this wind stress. In this section we will expand the previous discussion by comparing the impact of hydrographic data with that of sea surface height data for the purpose of reconstructing the cross-ridge heat transports and wind forcing.

As was indicated from the distribution of optimal observations in Fig. 3, February GSR heat transport anomalies leave a distinct down stream trace in the temperature field. The adjoint method in principle transforms this information into wind stress improvements. However, results from the previous section demonstrate that the monthly transport can not be fully recovered when missing convective adjustment prevents the transfer of information from the deep ocean to the surface. In contrast, sea surface hight (SSH) observations represent a surface signature of the underlying circulation and do not suffer from this restriction.

In the following we use daily SSH data to reconstruct the February 1990 heat transport. The result of the optimization is shown in Fig. 7, again as heat transport differences versus cost $\boxed{\text{Fig. 7}}$ function values. The figure shows that the heat transport can be reconstructed almost perfectly with a relation between heat transport error and cost function misfit that is almost linear. Note

that only a small reduction of the SSH misfit is associated with an almost correct estimation of the heat transport. Only monthly mean corrections of the surface fluxes are estimated so that only the monthly mean part of the SSH variability can be expected to be matched.

SSH observation that are optimal for reconstructing the February cross-ridge heat transport are shown in Fig. 8. The overflow temperature signal visible in Fig. 4 to emerge from the DS and the FB channel is now clearly visible as a sea level depression pulse that travels around the Cape Farewell and the Rikjanes Ridge (compare also discussion in Biastoch et al. (2002). Equally important is the positive signal along the eastern boundary, especially in the first month, where it reflects the density anomalies brought in by changes of the initial condition as shown in Fig. 3. The positive anomaly subsequently propagates northward and reaches across the GIN sea as a consequence of the anti-cyclonic barotropic circulation in that part of the basin. Obviously physical processes which are represented by hydrographic data have a corresponding signature in the SSH data. However, SSH fields SSH data have a closer link to wind stress data than hydrographic observations and constrain the estimation of the wind stress with the adjoint method much more efficiently.

Fig. 8

8. Conclusion

The design of a climate observing system is an important element of ocean state estimation. In contrast to existing approaches that use adjoint sensitivities, the design problem was discussed here in the context of optimal observations that emerge as singular vectors from the observability matrix. It was shown that in the limit of large observational errors, an

approximation of optimal observations for scalar quantities can be calculated essentially by one run of the adjoint and one additional forward run of the linearized forward model. Although the limits of large observational errors rarely apply, the observations calculated for this limit were shown to apply equally well beyond the limit.

An important result, obtained here for the example of reconstructing the heat transport across the GSR, is that optimal observations are most efficient in constraining the optimization problem and in particular perform significantly better than can be achieved by using section data or even basin wide data. This is counter-intuitive but can be understood in that those additional data, while not carrying more information about the GSR heat transport, do complicate the shape of the cost function and thus degrade the performance of the procedure. For understanding the sampling problem of the ocean this is an important result: well selected observations seem significantly more valuable than random coverage. However, while interpreting this result we have to recall that it represents our model (identical twin) simulation and there only the specific question of the GSR heat transport. The corollary would be: determining optimal observations for a particular phenomenon in an imperfect model could prove not to be the optimal basis for observing the real world.

Another important result is that in our context of the GSR heat transport estimates, SSH data provide more robust information than hydrographic data at least on shorter time scales. The reason is that different dynamical regimes may be represented in the data than in the model first guess which in turn may reduce the value of hydrographic data for the estimation of surface flux fields required to reconstruct the GSR heat transport. This was shown to hold due

to convective adjustment, but can be expected to be the case also for many other processes. Therefore optimal observations have to be used with care since they describe only local properties and do not guaranty skill for the estimation of the quantity they are designed for, even though they may represent the associated physical processes well.

We note that optimal observations describe causes and effects of anomalies of a scalar quantity and in general show a quite complex structures. In case of the GSR heat transport, the pathways of the overflow water through the DS and FB channel is clearly emphasized in the position of optimal observations. Those hydrographic conditions are also reflected in the sea level fields as negative gradient signal which is related to a SSH depression ' pulse that travels around Cape Farewell. Although not all details may necessarily be resolved in a survey, their values is apart from identifying key regions in providing a new tool for studying the causes and effects of anomalies of integral quantities.

Little may have been learned here regarding optimal observations for the GSR heat transport since mainly expected features of the circulation were revealed and because we limited our experiments to only one year. However, we consider the value of the present work to be in providing confidence in the validity of their structures and their ability to emphasize physical processes associated with anomalies of certain scalar quantities.

Consortium for Estimating the Circulation and Climate of the Ocean (ECCO) funded by the

National Oceanographic Partnership Program.

References

Adcroft, A., C. Hill, and J. Marshall, 1997: Representation of topography by shaved cells in a height coordinate ocean model, *MWR*, **125**, 2293–2315.

Bacon, S., 1998: Decadal variability in the outflow from the Nordic seas to the deep Atlantic Ocean, *Nature*, **394**, 871–874.

Barth, N., and C. Wunsch, 1990: Oceanographic experiment design by simulated annealing, *JPO*, **20**, 1249–1263.

Biastoch, A., R. Käse, and D. Stammer, 2002: Mass and heat exchange across the Greenland-Scotland Ridge, *J. Phys. Oceanogr.*, submitted.

Dickson, B., I. Yashayaev, J. Meincke, and B. Turrell, 2002: Rapid freshening of the deep North Atlantic Ocean over the past four decades, *Nature*, **416**, 832–836.

Dickson, R. R., and J. Brown, 1994: The production of North Atlantic deep water: Sources, rates and pathways, *J. Geophys. Res.*, **99**, 12,319–12,341.

ETOPO5, 1988: Digital relief of the surface of the earth. worldwide bathymetry/topography data announcement 88-mgg-02, *Technical report, National Geophysical Data Center*.

Fu, L.-L., and A. Cazenave, 2001: *Satellite Altimetry and Earth Sciences: A Handbook for Techniques and Applications*, Academic Press, San Diego.

Fukumori, I., 2001: *Data assimilation by models.*, Academic, San Diego, 237–266, Satellite Altimetry and Earth Sciences.

Giering, R., and T. Kaminski, 1998: Recipes for Adjoint Code Construction, *ACM Trans. On Math. Software*, **24**, 437–474.

Gilbert, J. C., and C. Lemaréchal, 1989: Some numerical experiments with variable-storage Quasi-Newton algorithms, *Math. Program.*, **45**, 407–435.

Hansen, B., and S. Østerhus, 2000: North Atlantic–Nordic Seas exchanges, *Prog. Oceanogr.*, **45**, 109–208.

Hansen, B., W. R. Turrell, and S. Østerhus, 2001: Decreasing overflows from the Nordic seas into the North Atlantic Ocean through the Faroe Bank channel scince 1950, *Nature*, **411**, 927–930.

Hurell, J. W., and H. van Loon, 1997: Decadal variations in climate associated with the Nort Atlantic Oscillation, *Climate Change*, **36**, 301–326.

Jerlov, N. G., 1968: *Optical Oceanography*, Elsevier, New York.

Käse, R., and A. Oschlies, 2000: Flow through denmark strait, *J. Geophys. Res.*, **10**, 28527–28546.

Kleeman, R., and A. M. Moore, 1997: A theory for the limitation of ENSO predictability due to stochastic atmospheric transients, *J. Atmos. Sci.*, **54**, 753–767.

Lee, T., I. Fukumori, D. Menemenlis, Z. Xing, and L.-L. Fu, 2002: Effects of the Indonesian Throughflow on the Pacific and Indian Oceans, *J. Phys. Oceanogr.*, **32**, 1404–1429.

Levitus, S., R. Burgett, and T. P. Boyer, 1994: World Ocean Atlas 1994, vol. 3, Salinity and vol. 4, Temperature, NOAA Atlas NESDIS 3, *U.S. Dep. Of Comm., D.C.*.

Marotzke, J. R. Giering, Q. K. Zhang, D. Stammer, C. N. Hill, and T. Lee, 1999: Construction of the adjoint MIT ocean general circulation model and application to Atlantic heat transport sensitivity, *J. Geophys. Res.*, **104**, 29,529–29,548.

Marshall, J., A. Adcroft, C. Hill, L. Perelman, and C. Heisey, 1997: A finite-voloume, incompressible Navier Stokes model for studies of the ocean on parallel computers, *J. Geophys. Res.*, **102**, 5753–5766.

Menke, W., 1989: *Geophysical data analysis : discrete inverse theory*, Academic Press, San Diego.

Paulson, C. A., and J. J. Simpson, 1977: Irradiance measurements in the upper ocean, *J. Phys. Oceanogr.*, **7**, 952–956.

Roemmich, D., and W. B. Owens, 2000: The Argo Project: Global ocean observations for understanding and prediction of climate variability., *Oceanography*, **13**, 45–50,.

Schröter, J., and C. Wunsch, 1986: Solution of nonlinear finite difference ocean models by optimization methods with sensitivity and observational strategy analysis, *J. Phys. Oceanogr.*, **16**, 1855–1874.

Stammer, D., K. Ueyoshi, W. Large, and C. Wunsch, 2002a: Surface fluxes estimated through ocean data assimilation, *J. Climate*, submitted for publication.

Stammer, D., and C. Wunsch, 1996: The determination of the large-scale circulation of the Pacific Ocean from satellite altimetry using Green's functions, *J. Geophys. Res.*, **101**, 18,409–18,432.

Stammer, D., C. Wunsch, R. Giering, C. Eckert, P. Heimbach, J. Marotzke, A. Adcroft, C. Hill, and J. Marshall, 2002b: The global ocean circulation during 1992 -1997, estimated from ocean observations and a general circulation model, *J. Geophys. Res.*, **107**.

Stammer, D., C. Wunsch, R. Giering, C. Eckert, P. Heimbach, J. Marotzke, A. Adcroft, C. Hill, and J. Marshall, 2002c: Volume, heat and freshwater transports of the global ocean circulation 1992 –1997, estimated from a general circulation model constrained by woce data, *J. Geophys. Res*, in press.

Wunsch, C., 1996: *The Ocean Circulation Inverse Problem*, Cambridge University Press, New York, Melbourne.
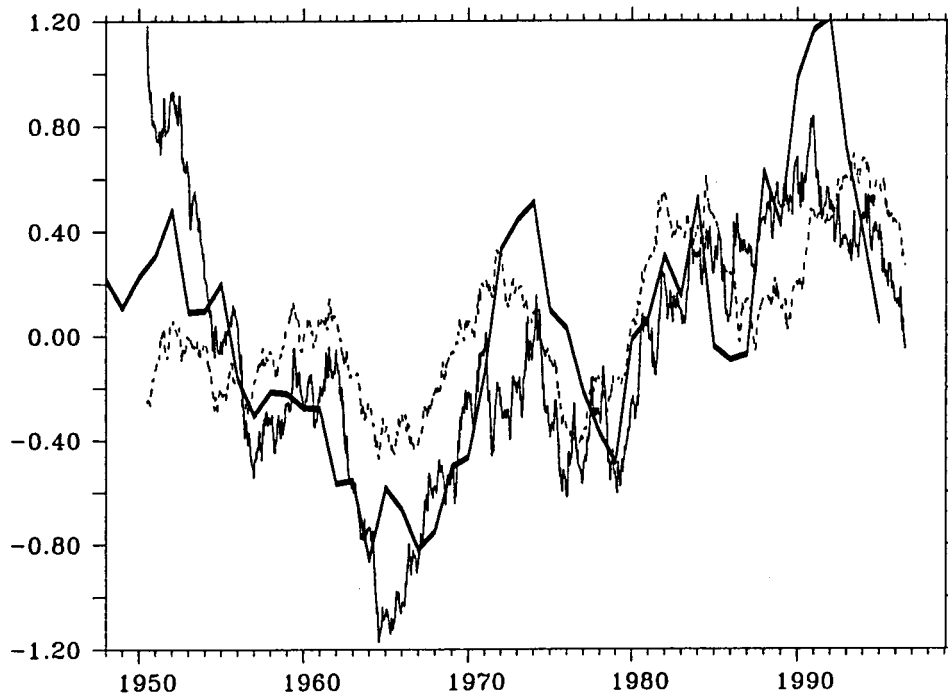
Figure 1. Anomalies of GS ridge heat transport (solid; in 10 TW), southward volume transport

through Denmark Strait channel (dashed; in $Sv=10^6$ m^3/s), and 0.5× NAO index (bold). All

three curves were smoothed with a 5 year running-mean to filter high-frequency fluctuations.

The remaining signal accounts for about 10% of the total variability. The mean heat transport

is 0.10 PW and the mean southward volume transport is 6.5 Sv.
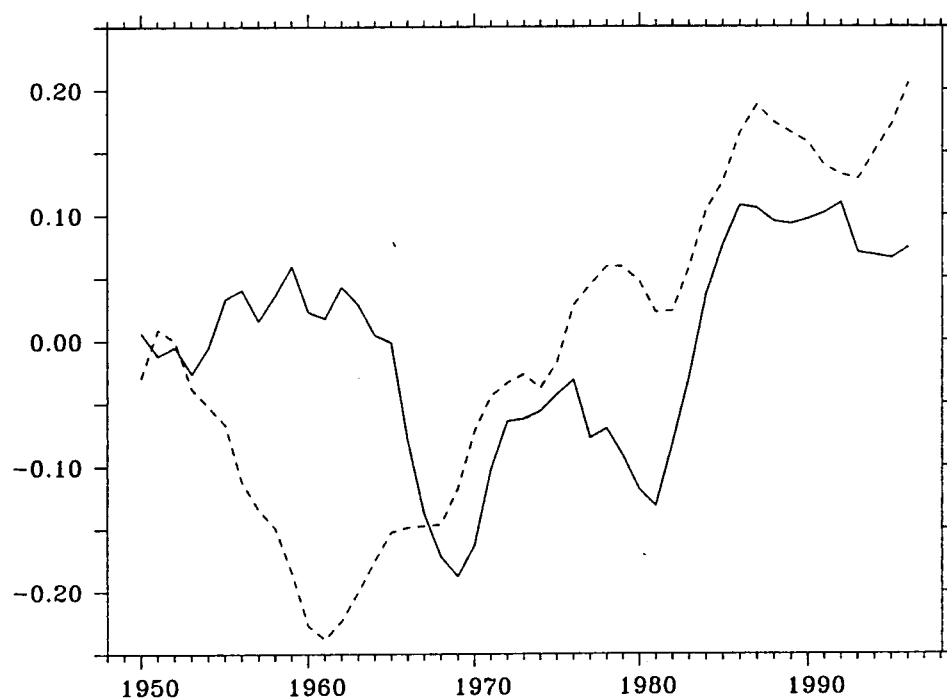
Figure 2. Anomalies of potential temperature θ (in ^{o}C) averaged vertically over the water column and over the model domain between 50-10°W; 60-66.75^{o}N (dashed), and 50-10°W; 66.75-70°N (solid). Both curves were smoothed with a 5 year running-mean filter to remove high-frequency fluctuations.
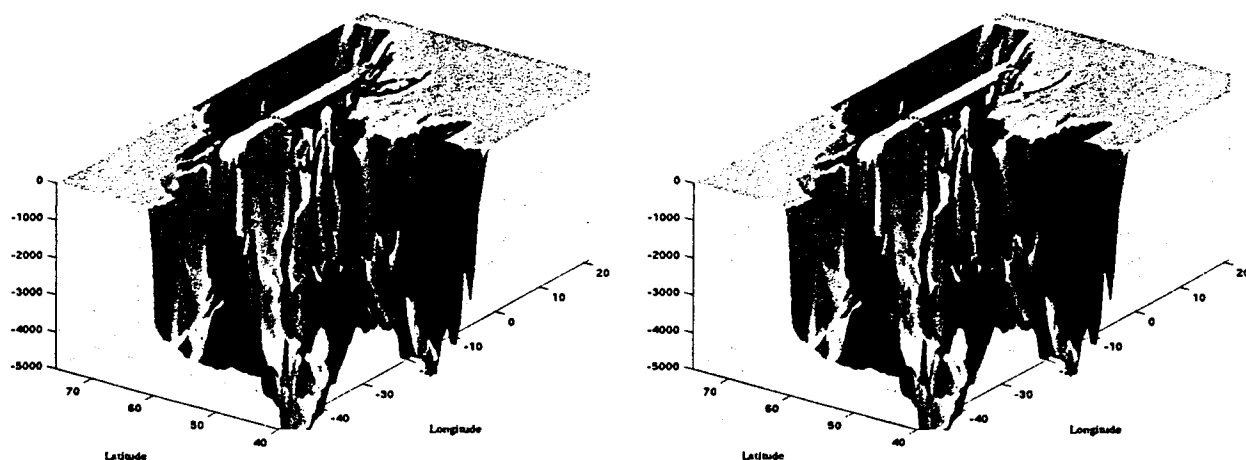
Figure 3. Sensitivity of February meridional heat transport across the GSR with respect to the January 1st temperature (left) and salinity (right) initial conditions. The section, across which the heat transport is calculated, is marked in yellow and blue. Regions with small sensitivities are excluded from the graph. The isosurface are at 0.67 TW/^{o}C and 2.0 TW/PSU for temperature and salinity, respectively.
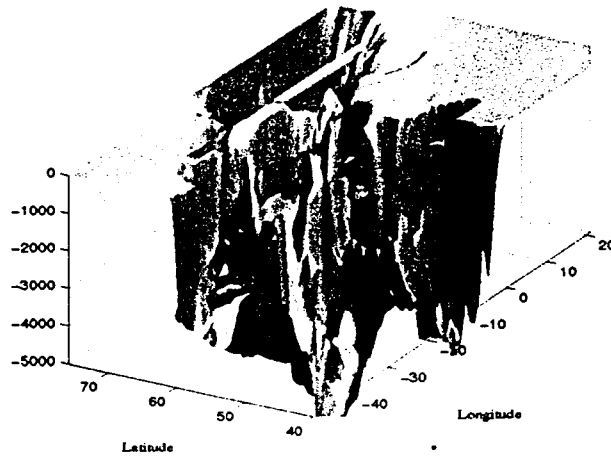
January
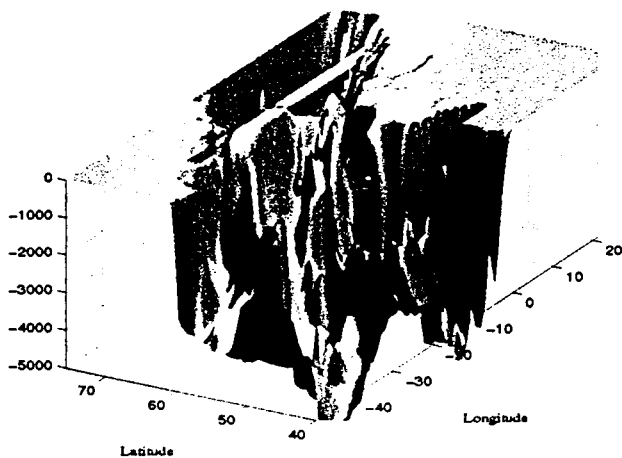
February
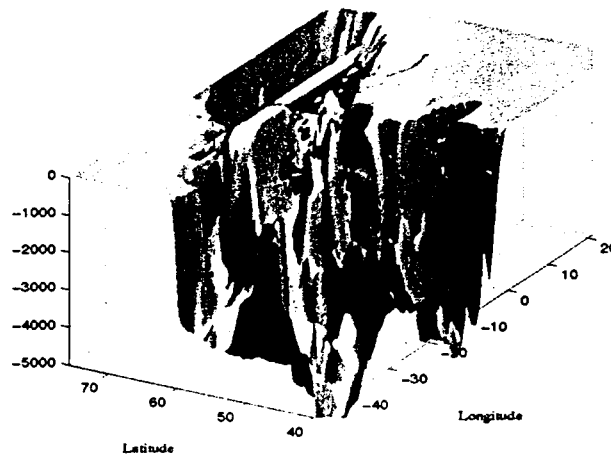
March
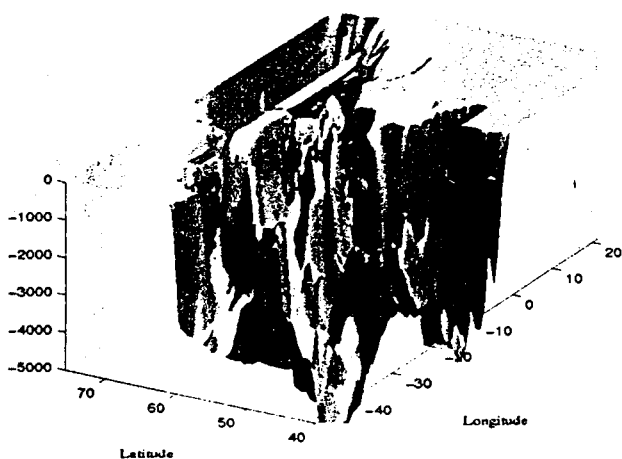
April
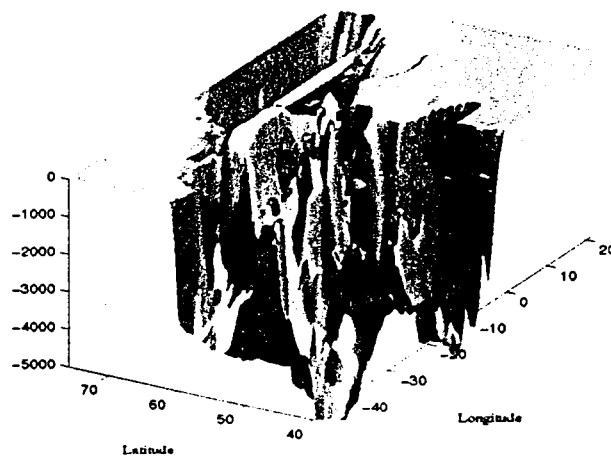
August
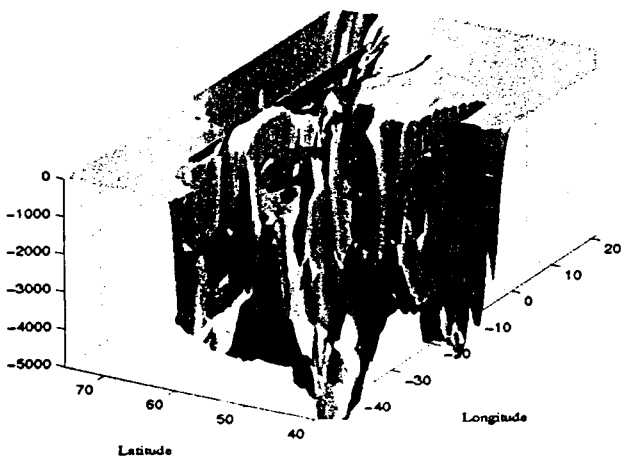
December

Figure 4. Location of hydrographic observations that are optimal for inferring February meridional heat transport across the GSR. Red and green surface are isosurfaces (positive and negative, respectively) of the nondimensionalized gradient of the heat transport with respect to temperature observations for different months. Regions without optimal observations, i.e., without any noticeable impact on the cost function, are not shown in the figure. The section is marked in yellow and blue.
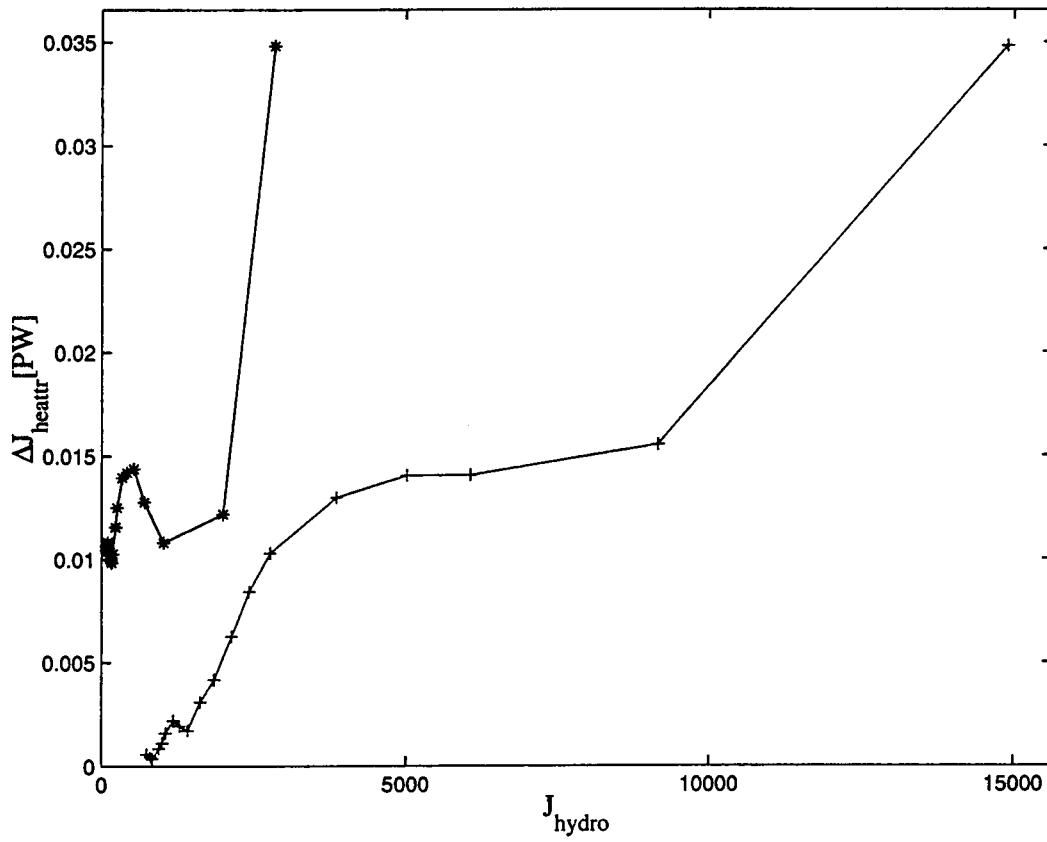
Figure 5. Annual mean heat transport difference ΔJ_{heattr} in dependence of the cost function decrease J_{hydro}. ΔJ_{heattr} is calculated with respect to the annual mean value of the simulation of Year 1990. First guess initial condition and daily/twice daily forcing correspond to year 1965. The use of monthly mean temperature and salinity along the section, the heat transport is defined, is denoted by '*'. The curve denoted by '+' corresponds to using same number of data points at optimal locations. Both optimizations were stopped after iteration 16.
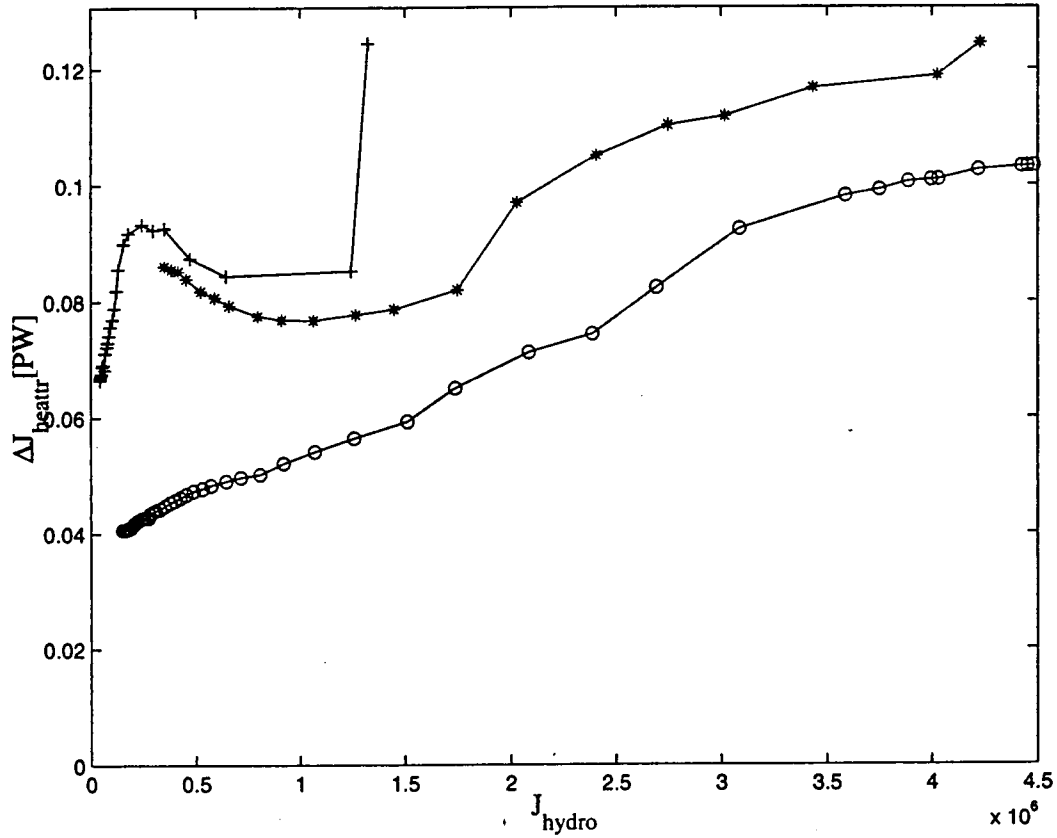
Figure 6. February heat transport difference year 90-65, ΔJ_{heattr}, in dependence of the cost

function decrease J_{hydro}. J_{hydro} comprises optimal salinity and temperature data. The curves

denoted with '+', '*', and 'o' correspond respectively to experiments using optimal (same no.

as on the GSR section) and all available monthly mean data for the standard setup and an
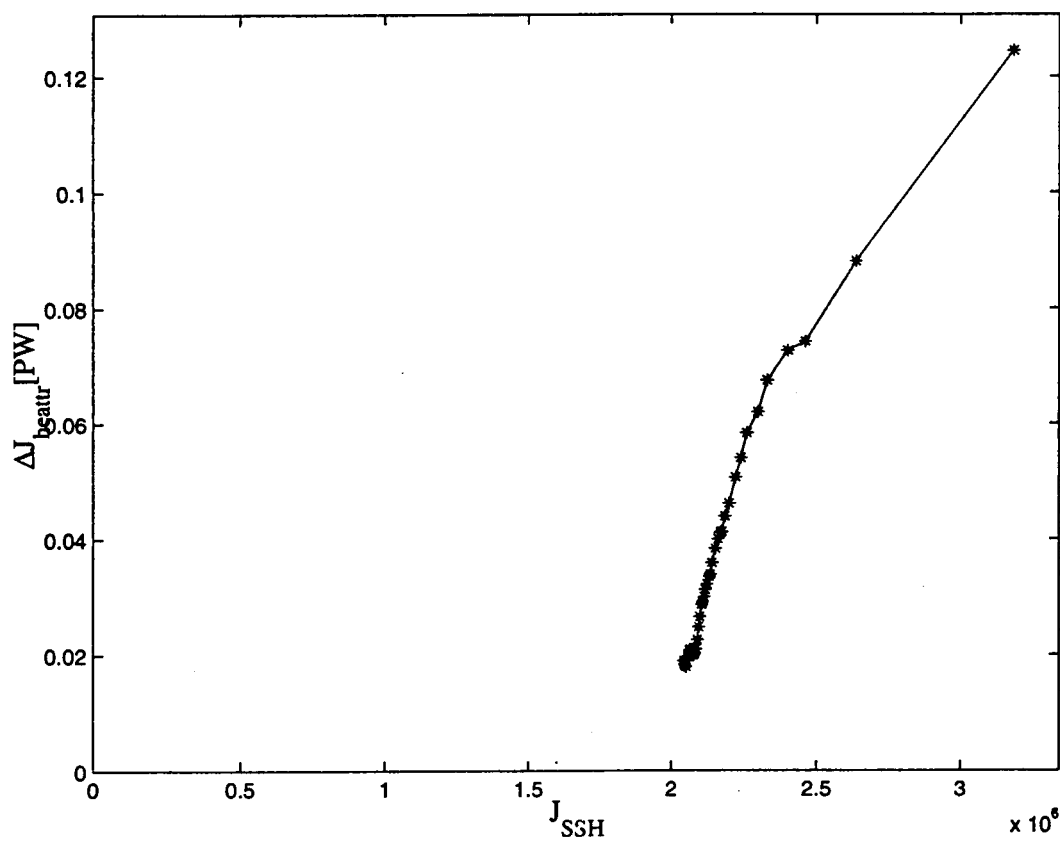
experiment without convective adjustment.

Figure 7. February heat transport difference year 90-65, ΔJ_{heattr}, in dependence of the cost function decrease J_{SSH}. J_{SSH} includes daily SSH data.
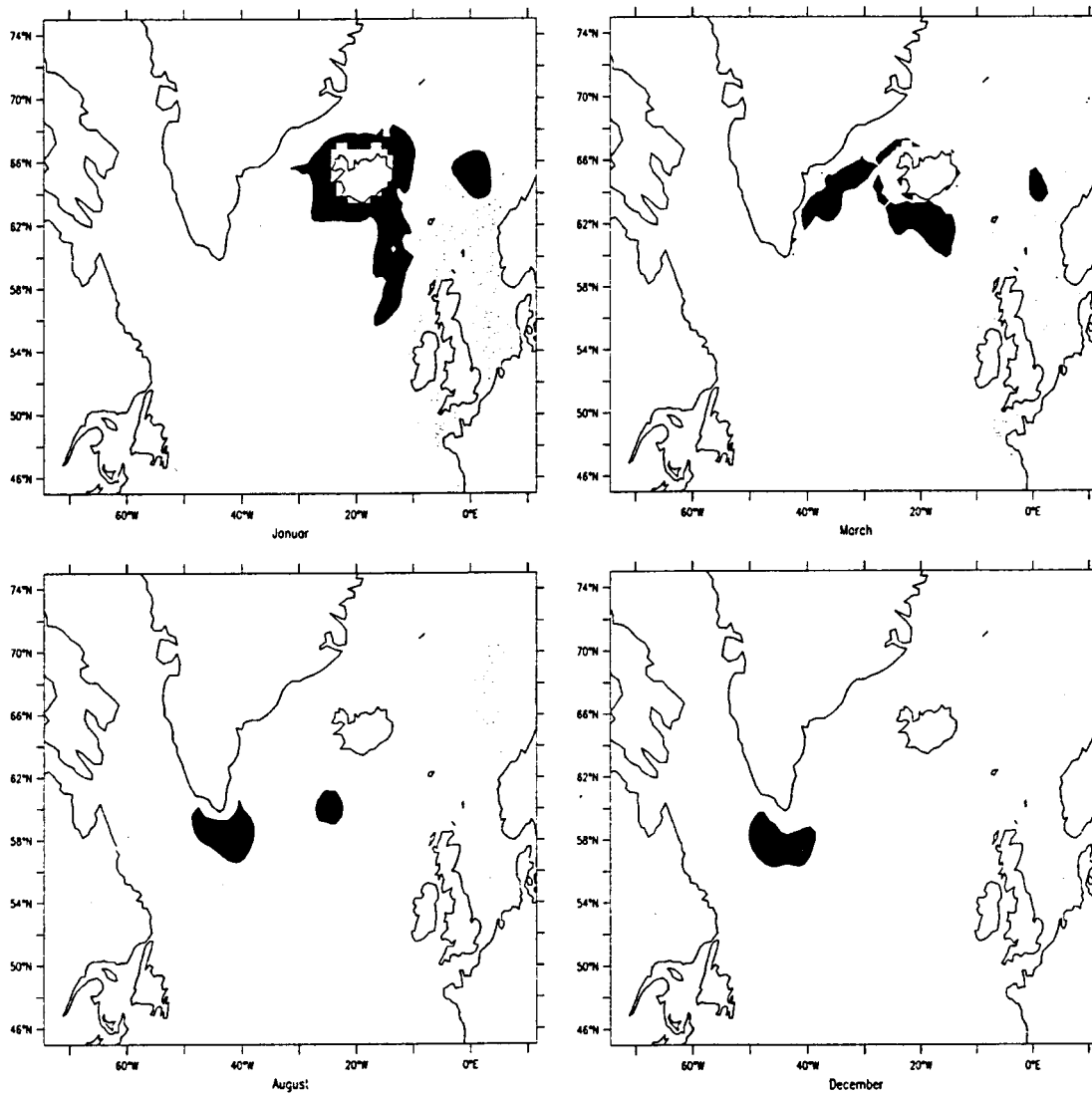
Figure 8. Gradient of the February meridional heat transport with respect to SSH observations.

Black and gray patterns correspond to negative and positive response of the sea surface. The

contours are at ± 2.1 TW/cm for a spatially uniform SSH error of 5 cm.